Natural Product Communications
Volume 17(8): 1–8

DOI: 10.1177/1934578X221114227
journals.sagepub.com/home/npx

(*R*)-13a*α*-Densiindolizidine, A New Phenanthroindolizidine Alkaloid From *Cryptocarya densiflora* Blume (Lauraceae) and Molecular Docking Against SARS-CoV-2

Wan N Nazneem Wan Othman[1], Fatimah Salim[1,2], Nor N Abdullah[1,2], Syahrul I Abu Bakar[1,2], Khalijah Awang[3], Lalith Jayasinghe[4] and Nor H Ismail[1,2,4]

Abstract

Cryptocarya densiflora Blume (Lauraceae) is an evergreen tree widely distributed throughout the hills and mountain forests up to 1500 m in Malaysia and Indonesia. The plant has been reported to contain phenanthroindolizidine-type of alkaloids. In the present work, a new phenanthroindolizidine alkaloid named (*R*)-13a*α*-densiindolizidine, was isolated from the dichloromethane (DCM) extract of the leaves. The structure of the alkaloid was established based on 1D and 2D nuclear magnetic resonance (NMR) and liquid chromatography mass spectrometry-ion trap-time of flight (LCMS-IT-TOF) analysis. (*R*)-13a*α*-densiindolizidine displayed binding interactions with crucial amino acid residues in the active sites of severe acute respiratory syndrome coronavirus 2 M^{pro} (SARS-CoV-2 M^{pro}) and RNA-dependent protease (RdRp) *in silico*, whilst fulfilling the absorption, distribution, metabolism, excretion, and toxicity (ADMET) criteria and Lipinsky's rule, thus revealing its potential as a lead compound.

Keywords

phenanthroindolizidine alkaloid, *Cryptocarya densiflora*, molecular docking, ADMET, SARS-CoV-2

Received: April 7th, 2022; Accepted: June 29th, 2022.

Introduction

Cryptocarya genus comprises around 200 to 250 plant species distributed across South China and India to North Australia, Madagascar, and South America, in which 17 species can be found in Peninsular Malaysia, including *Cryptocarya densiflora* Blume.[1] The species *C densiflora* is a medium sized tree, up to 20 m in height and 135 cm in girth.[2] Although several *Cryptocarya* species are known for traditional medicine such as for women after childbirth and treating diarrhea,[3] however, none is known for *C densiflora*. Phytochemically, *Cryptocarya* species have been reported to contain flavonoids,[4] pyrones,[5] lignans,[6] chalcones,[7] and alkaloids.[8] Several phenanthroindolizidine alkaloids have been isolated from *Crytocarya* species including three from *C densiflora* from our previous work.[9,10]

Phenanthroindolizidine alkaloids are known to exhibit interesting pharmacological properties.[11] Apart from *Cryptocarya* genus, these alkaloids are present in a few species of Asclepiadaceae, Acanthaceae, and Moraceae families.[12] Since the first isolation of tylophorine in 1935,[13] phenanthroindolizidine alkaloids have attracted much attention because they exhibited antitumor and anticancer activity, as well as inhibitors of protein synthesis.[14] More than 100 natural phenanthroindolizidines have been reported to date. Antofine has been extensively studied towards the development of potent anticancer agent due to its excellent cytotoxic activity.[14,15] In addition, several phenanthroindolizidine alkaloids such as tylophorine, tylophorinine and 7-methoxycryptopleurine have been reported to display potency against SARS-CoV-2 and transmissible gastroenteritis

[1]Atta-ur-Rahman Institute for Natural Products Discovery, Universiti Teknologi MARA, Bandar Puncak Alam, Selangor, Malaysia
[2]Faculty of Applied Sciences, Universiti Teknologi MARA, Shah Alam, Selangor, Malaysia
[3]Department of Chemistry, Faculty of Science, University of Malaya, Kuala Lumpur, Malaysia
[4]National Institute of Fundamental Studies, Kandy, Sri Lanka

Corresponding Author:
Nor H Ismail, Atta-ur-Rahman Institute for Natural Products Discovery, Universiti Teknologi MARA, Puncak Alam Campus, 42300 Bandar Puncak Alam, Selangor, Malaysia.
Email: norhadiani@uitm.edu.my

virus (TGEV) *in vitro* at low nanomolar level with high oral availability in rats. These suggested they could be used as potential therapeutic agents for coronavirus infections.[16–18]

This paper describes the isolation and characterization of a new phenanthroindolizidine alkaloid, (*R*)-13aα-densiindolizidine, from the DCM extract of the leaves of *C densiflora*. Inspired by the pharmacological properties of previously reported phenanthroindolizidines, we evaluated the binding interactions of (*R*)-13aα-densiindolizidine with important amino acid residues in the active sites of SARS-CoV-2 M^{pro} and RdRp *in silico*, as well its drug-likeness properties.

Results and Discussion

The new alkaloid (Figure 1) was obtained as an optically active dark brownish amorphous solid with $[\alpha]_D^{25} - 115°$ ($c = 1.1$, MeOH). It was assigned the molecular formula of $C_{22}H_{23}NO_3$ with 12 degrees of unsaturation through LCMS-IT-TOF analysis $[M+H]^+$, m/z 350.1759 (calcd. for $C_{22}H_{24}NO_3$, 350.1751). The ultraviolet (UV) spectrum exhibited characteristic absorption peaks of phenanthroindolizidine moiety at λ_{max} 252, 265, 281, 340, and 355 nm.[19] The infrared (IR) spectrum revealed absorption bands due to hydroxy (OH) and aromatic (C=C) functional groups at ν_{max} 3340, 1596, and 1519 cm^{-1}, respectively. The ^1H NMR spectroscopic data (Table 1) showed two mutually coupled doublets at δ_H 7.66 (1H, d, $J = 9.0$ Hz) and 7.23 (1H, d, $J = 9.0$ Hz) which were assigned to H-1 and H-2 of ring A, as a ^1H-^1H correlation spectroscopy (COSY) (Figure 2) was observed between H-1 and H-2. In addition, a broad singlet was assignable to H-5 appeared at δ_H 9.03 (1H, brs) and two broad doublets at δ_H 7.06 (1H, brd, $J = 7.8$ Hz) and 7.51 (1H, brd, $J = 7.8$ Hz) were attributed to H-7 and H-8, respectively, of the aromatic ring C. The position of the methoxyls at δ_H 3.96 and 3.81 was assigned to C-3 and C-4, respectively, based on the heteronuclear multiple bond correlations (HMBC) (Figure 2) of H-2/OCH_3-3, H-1/C-3, 3-OCH_3/C-3, H-2/C-4, and 4-OCH_3/C-4. Further analysis of the COSY experiment (Figure 2) showed all the correlations of vicinal protons; H-1/H-2, H-8/H-7, H-11/H-12, H-12/H-13, H-13a/H-13, and H-14/H-13a in the structure. The combined analysis of the ^{13}C NMR (Table 1) and the distortionless enhancement by polarization transfer (DEPT) spectra confirmed the presence of 22 carbon resonances comprising five aromatics, two methoxyls, one methine, five methylenes, and nine quaternaries which further support the proposed molecular formula. These NMR data closely resembled those of ficuseptine D,[20] except for the absence of 6-OCH_3 resonance. Further inspection of the ^1H and ^{13}C NMR resonances indicated the presence of a hydroxy group in ring C, as suggested by the LCMS-IT-TOF data and IR spectrum. The hydroxy group was assigned to C-6. Comparison of the ^1H NMR shift observed for the H-13a axial ficuseptine D allowed for the assignment of the H-13a in the present alkaloid as an axial. The proposed α orientation was confirmed by the nuclear overhauser effect spectroscopy (NOESY) correlations of H-13a with H-9α and 14α, indicating their cofacial proximity (Figure 3). Phenanthroindolizidines type of alkaloid was previously isolated from *C chinensis* and *C phyllostemon* and the absolute configuration at C-13a has been established as *R* from its

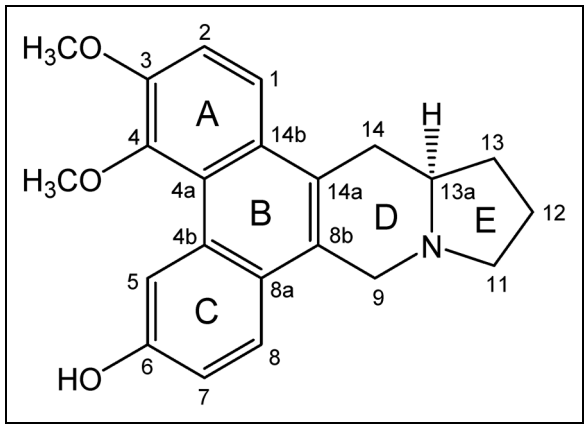

Figure 1. Molecular structure of (*R*)-13aα-densiindolizidine.

Table 1. ^1H and ^{13}C NMR Spectroscopic Assignments of (*R*)-13aα-Densiindolizidine in $CDCl_3$.

Position	δ_H (ppm), J (Hz)	δ_C (ppm)	COSY	HMBC	NOESY
1	7.66 (d, 9.0)	112.9	H-2	C-3, 4a	H-14α
2	7.23 (d, 9.0)	119.4	H-1	C-3, 4, 14b	3-OCH_3
3	—	150.7			
4	—	147.1			
4a	—	123.6			
4b	—	130.0			
5	9.03 (brs)	112.7		C-7, 8a	4-OCH_3
6	—	154.6			
7	7.06 (brd, 7.8)	116.6	H-8		
8	7.51 (brd, 7.8)	123.2	H-7	C-4b, 6	H-9α
8a	—	124.8			
8b	—	125.7			
9	$\alpha = 4.60$ (d, 15.4) $\beta = 3.64$ (m)	53.3		C-13a, 14a	
11	$\alpha = 3.51$ (m) $\beta = 2.51$ (m)	54.7	H-12		
12	$\alpha = 1.98$ (m) $\beta = 2.04$ (m)	21.4	H-11, 13	C-13	
13	$\alpha = 2.25$ (m) $\beta = 1.81$ (m)	30.8	H-12, 13a	C-14	
13a	2.55 (m)	60.3	H-13, 14		H-9α, 14α
14	$\alpha = 2.93$ (brt, 11.3) $\beta = 3.26$ (brd, 15.0)	32.9	H-13a		
14a	—	125.2			
14b	—	127.8			
3-OCH_3	3.96 (s)	56.4		C-3	
4-OCH_3	3.81 (s)	59.8		C-4	

Abbreviations: s, singlet; d, doublet; brs, broad singlet; brd, broad doublet; brt, broad triplet; m, multiplet.

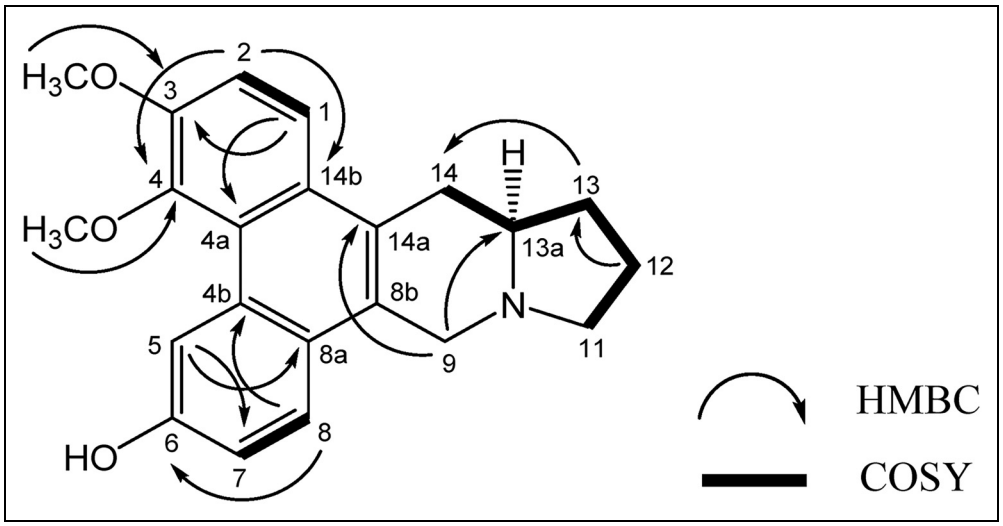

Figure 2. Key HMBC and COSY correlations of (*R*)-13a*α*-densiindolizidine.

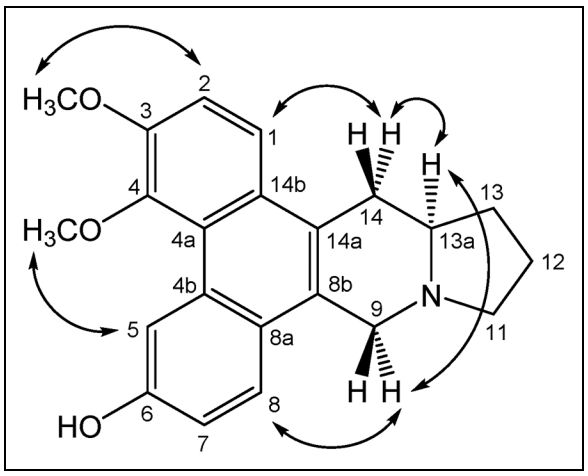

Figure 3. NOESY correlations of (*R*)-13a*α*-densiindolizidine.

circular dichroism (CD) spectrum analysis.[21,22] Thus, based on the structure elucidation and chemical correlation with phenanthroindolizidines type of alkaloid previously reported, the assignments thereby establishing the present alkaloid as (*R*)-13a*α*-densiindolizidine. The assignments of the proton and carbon resonances are tabulated in Table 1.

Lipinski's Rule

The physicochemical properties for (*R*)-13a*α*-densiindolizidine were predicted using SwissADME. A total of eight descriptors were taken into consideration (Table 2). Based on the result, (*R*)-13a*α*-densiindolizidine can be considered as a potential lead compound that obeys Lipinski's rule with good pharmacokinetic properties. (*R*)-13a*α*-densiindolizidine passed ADMETsar criteria for druggability as indicated in Table 3.

Molecular Docking Studies

The alkaloid (*R*)-13a*α*-densiindolizidine was subjected to docking studies against potential targets, SARS-CoV-2 protease M^{pro} (PDB ID: 6LU7), and RdRp (PDB ID: 7D4F). Based on the docking results, this alkaloid was able to fit in the substrate-binding pocket and binds to one of catalytic triad residue, Cys145, with docking interaction energy of −33.5 kcal/mol (Table 4). (*R*)-13a*α*-densiindolizidine was observed to form interactions with substrate binding sites (Glu166 and Thr190). The binding mode of (*R*)-13a*α*-densiindolizidine within the SARS-CoV-2 M^{pro} cavity is shown in Figure 4 whereby four hydrogen bonds were observed. Among these hydrogen bonds, a conventional hydrogen bond (O-H---N-H) between 6-hydroxyl group of the (*R*)-13a*α*-densiindolizidine with amino group (NH) from the residue Glu166 was the shortest distance (2.02 Å). The 3-methoxy group of (*R*)-13a*α*-densiindolizidine displayed the ability to form two carbon hydrogen bonds (C = O---H-C-O) with the oxygen from carboxylic acid group Thr190 residue (2.69 and 3.09 Å) and carbon-hydrogen bond interaction with amino acid residue Pro168 (2.73 Å) to strengthen the ligand-enzyme complex. The complex also participated in hydrophobic interaction between the sulfur of the Cys145 thiol group (SH) with one of the hydrogen at the E ring of (*R*)-13a*α*-densiindolizidine. This suggests that (*R*)-13a*α*-densiindolizidine is able to fit in the substrate-binding pocket and the interactions with the catalytic active residues are expected to enhance inhibition activity of the enzyme and prevent replication process of SARS-CoV-2.

In the development of the drug targets for SARS-CoV-2, RdRp protein play an important role due to the nonsimilar enzyme in host cell homologs, fewer off-targets effects against human host proteins, and development of selective SARS-CoV-2 RdRp inhibitors.[23] This enzyme has two binding sites including RNA template strand and RNA

Table 2. Physicochemical Properties Prediction for (*R*)-13a*α*-Densiindolizidine.

Ligand	Log $P_{o/w}$	MW[a]	TPSA[b]	Volume	Natoms[c]	HBA[d]	HBD[e]	Nrotb[f]
(*R*)-13a*α*-densiindolizidine	3.71	349.43	41.93	323.07	26	4	1	2

Abbreviations: MW, molecular weight (acceptable range: < 500); TPSA, topological polar surface area; Natoms, number of nonhydrogen atoms; HBA, number of hydrogen bond acceptors; HBD, number of hydrogen bond donors; Nrotb, number of rotatable bonds.

Table 3. Predicted ADMET Properties for (*R*)-13a*α*-Densiindolizidine.

Properties	Models	(*R*)-13a*α*-densiindolizidine
Physicochemical	Solubility (log S)	−4.97 (moderately soluble)
Absorption	P-glycoprotein inhibitor	Noninhibitor
	P-glycoprotein substrate	Nonsubstrate
	HIA	HIA +
	BBB	BBB +
Distribution	Gastrointestinal absorption	High
	CYP1A2 substrate	Substrate
Metabolism	CYP3A4 substrate	Substrate
	CYP2C9 substrate	Nonsubstrate
	CYP2C19 substrate	Nonsubstrate
	CYP2D6 substrate	Substrate
	CYP1A2 inhibitor	Inhibitor
	CYP3A4 inhibitor	Noninhibitor
	CYP2C9 inhibitor	Noninhibitor
	CYP2C19 inhibitor	Noninhibitor
	CYP2D6 inhibitor	Inhibitor
	heRG Inhibition	Inhibitor
Toxicity	H-HT	HHT +
	AMES mutagenicity	Nonmutagen
	Skin sensitization, (r) LLNA	Nonsensitizer
	DILI	DILI-

Abbreviations: CYP2D6, cytochrome P450 2D6; HIA, human intestinal absorption; BBB, bloodbrain barrier permeability; H-HT, human hepatotoxicity; DILI, drug induced liver injury.

primer strand (located near to RdRp catalytic site). Yin et al[24] reported that ligand suramin can inhibit the SARS-CoV-2 RdRp at these two binding sites. Residues Asn497, Lys500, Arg569, Gln573, Asn496, Lys577, Gly590, Leu576, Ala580, Ala685, Tyr689, and Leu758 were reported to interact with suramin in the RNA template strand binding site while residues Arg555, Lys551, Arg553, Arg836, Ala550, Lys551, Arg865, His439, Ile548, Ser549, Ala840, Ser861, and Leu862 are crucial amino acids for RNA primer strand.[24] Thus, any close interaction with these residues will disrupt the function of the RdRp protease. The result showed that the alkaloid (*R*)-13a*α*-densiindolizidine fits well in the RNA template and RNA primer strands binding sites with docking energy value of −29.9 and −27.1 kcal/mol, respectively.

In the case of RNA template strand binding site shown in Figure 5, alkaloid (*R*)-13a*α*-densiindolizidine displayed the ability to interact with active residues Lys500, Asn496, Leu576, Ala580, Lys577, and Ala685. Interaction with these residues is expected to block the binding site of RNA template strand, thus inhibiting RdRp activity. The ligand-enzyme complex was stabilized by a conventional hydrogen bond between oxygen from 6-hydroxyl group of (*R*)-13a*α*-densiindolizidine and amino group (NH) of the residue Lys500 (2.05 Å). Alkaloid (*R*)-13a*α*-densiindolizidine can be potentially stabilized by carbon-hydrogen bond interactions (C = O-----H-C) between oxygen from carbonyl group of Leu576 (2.39 and 2.68 Å) and hydrogen of the C-11 methylene of (*R*)-13a*α*-densiindolizidine. In addition, the hydrogen of the C-9 of (*R*)-13a*α*-densiindolizidine has the potential to form carbon-hydrogen bond interaction (C = O---H-R) with oxygen from the carbonyl functional group on residue Asn496. The alkaloid was further stabilized by hydrophobic interaction with residues Ala580 and Lys577 and π-alkyl interaction with residue Ala685.

The alkaloid (*R*)-13a*α*-densiindolizidine was also predicted to be able to fit in the RNA primer strand binding site (Figure 6) through several hydrogen bonds and electrostatic interactions. This alkaloid binds to the enzyme through four conventional hydrogen bond interactions which include (1) oxygen of 3- and 4-methoxy groups (R-O---H-N) with the hydrogen of amino group Lys545 residue (2.05 Å); (2) oxygen of 4-methoxy group (N-H---O-R) with hydrogen from amino group (NH) of Arg555 residue; (3) 6-hydroxyl group (N-H---O-H) with hydrogen of amino group from the Arg555. This ligand-protease complex was further stabilized through electrostatic π-cation interaction of rings A, B, and C of the alkaloid with Arg555. Overall, (*R*)-13a*α*-densiindolizidine was observed to display potential binding interactions with the catalytic triad of SARS-CoV-2 M^{pro} and can potentially act as inhibitor of SARS-CoV-2 RdRp by blocking both crucial binding sites, the template and primer strands of RdRp.

Experimental

General

Analytical and preparative thin-layer chromatography (TLC) was carried out on Merck 60 F_{254} silica gel plates (absorbent thickness: 0.25 and 0.50 mm, respectively). Column chromatography (CC) was performed using silica gel (Merck 230-400 mesh, ASTM). Ultraviolet (UV) spectra were recorded using a Shimadzu UV-250 UV–Visible Spectrophotometer. IR spectra were recorded using a Perkin-Elmer Spectrum 400 FT-IR Spectrometer. NMR spectra were acquired in deuterated chloroform ($CDCl_3$) (Merck) with tetramethylsilane (TMS) as the internal standard

Table 4. Docking Interaction of (*R*)-13aα-Densiindolizidine Against SARS-CoV-2 M^{pro} and RdRp.

Protein	CDOCKER Interaction energy (-kcal/mol)	Hydrogen bond interaction	Hydrophobic interaction	π-interaction	
		Residues/distance (Å)	Residues/distance (Å)	Residues/distance (Å)	Type of interaction
M^{pro}	33.5	Glu166 (2.02) Thr190 (2.69) Thr190 (3.09) Pro168 (2.73)	Cys145 (4.71)	Glu166 (3.18) Glu166 (3.70)	π-donor H-bond π-anion
RdRp template strand	29.9	Lys500 (2.06) Leu576 (2.39) Leu576 (2.68) Asn496 (3.04)	Ala580 (4.17) Lys577 (4.54)	Ala685 (3.92) Ala685 (5.19)	π-alkyl π-alkyl
RdRp primer strand	27.1	Lys545 (2.05) Lys545 (2.05) Arg555 (2.40) Arg555 (3.00)	—	His439 (4.54) His439 (5.37) Arg555 (4.41) Arg555 (4.69) Arg555 (4.93)	π-alkyl π-alkyl π-cation π-cation π-cation

using the BRUKER Avance III 400 MHz NMR and BRUKER Avance III 600 MHz NMR spectrometers. Chemical shifts are given in the δ scale. LCMS-IT-TOF spectra were obtained using an Agilent Technologies 6530 AccurateMass Q-TOF LC/MS system. A Jasco P1020 polarimeter was used to measure optical rotation. All solvents were of analytical grade and were distilled prior to use.

Plant Materials

The leaves of *C densiflora* was collected from Hutan Simpan Tembat, Ulu Terengganu, Terengganu, Malaysia and were authenticated by a certified botanist, Teo Leong Eng, Department of Chemistry, Faculty of Science, University of Malaya. A voucher specimen (KL 5211) has been deposited with the University of Malaya herbarium.

Extraction and Isolation

Plant extraction was carried out by cold percolation. Dried grounded leaves of *C densiflora* (2.5 kg) was first defatted with hexane (15 L) for three days at room temperature. The resulting slurry was filtered, and the residual plant material was moistened with 25% ammonia solution (1 L) and left for two hours to aggregate the nitrogen-containing compounds in the plant. The basified residual plant material was then successively reextracted with DCM (15 L, 3×). The DCM extract was repeatedly extracted with a solution of 5% hydrochloric acid (0.5 L, 1×) until it gave a negative result for Mayer's test. It was next basified with 25% ammonia solution to about pH 11 and reextracted with DCM (3 L, 1×) to yield 13 g of extract. The DCM crude extract was subjected to exhaustive CC over silica gel and eluted with DCM which was gradually enriched with methanol (MeOH). The ratio of the solvent between DCM and MeOH were (100:0; 99:1; 98:2; 97:3; 96:4; 95:5; 94:6; 93:7; 92:8; 90:10; 85:15; 80:20, and 50:50). Fractions were collected every 100 mL and each fraction was tested with aluminum TLC plate for their alkaloids. The alkaloid spots were first detected by UV light (254 and 366 nm) and confirmed by spraying with Dragendorff's reagent. Fraction having spots with the same R_f values and stains were combined and treated as a group. The combined groups were purified with CC and preparative TLC. Isolation and purification (13 g) of alkaloid yielded 20 fractions. Further purification of fraction F7 by a preparative TLC using DCM: MeOH with 97:3; *v*/*v*, saturated with ammonium hydroxide (NH_4OH); gave (*R*)-13aα-densiindolizidine.

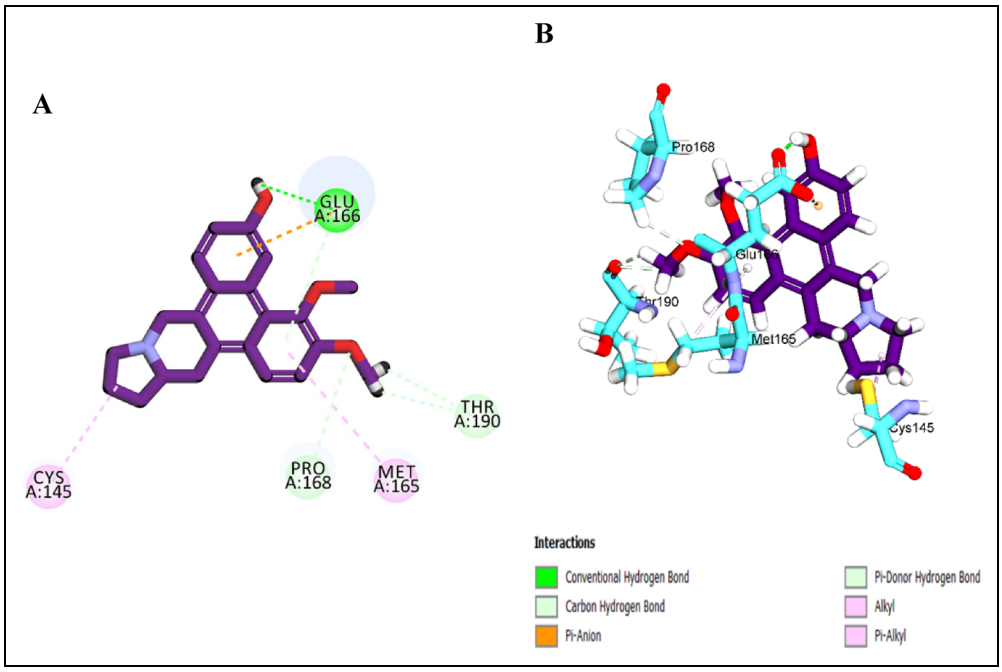

Figure 4. (A) 2D interaction of (*R*)-13aα-densiindolizidine with SARS-CoV-2 M^{pro} protein; (B) 3D interaction of (*R*)-13aα-densiindolizidine with SARS-CoV-2 M^{pro} protein.

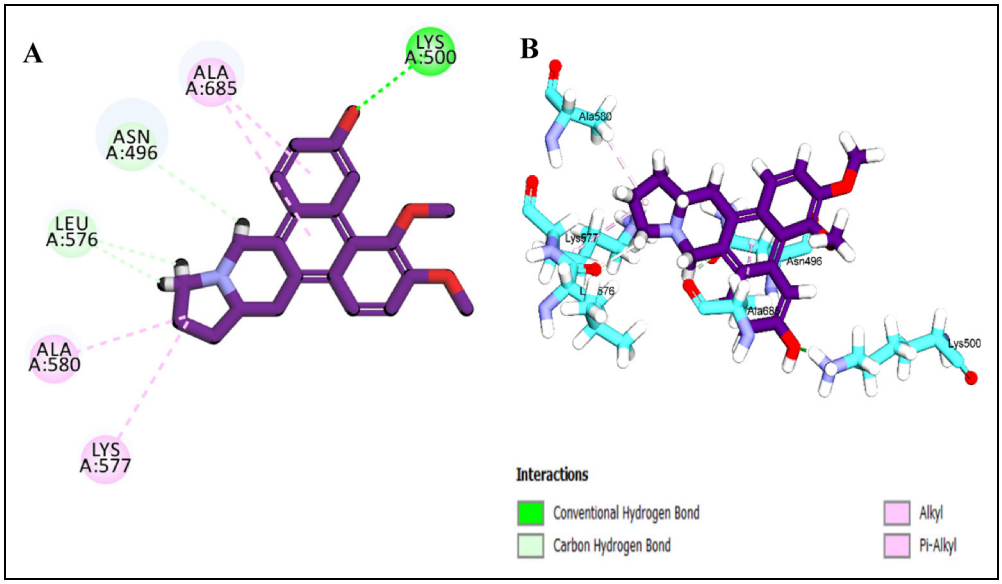

Figure 5. (A) 2D interaction of (*R*)-13aα-densiindolizidine at RNA template binding site of SARS-CoV-2 RdRp protein; (B) 3D interaction of (*R*)-13aα-densiindolizidine at RNA template binding site SARS-CoV-2 RdRp protein.

(*R*)-13aα-densiindolizidine: dark brownish amorphous solid; $[\alpha]_D^{25} -115°$ ($c = 1.1$, MeOH); LCMS-IT-TOF m/z: 350.1759 $[M+H]^+$ (calcd. for $C_{22}H_{24}NO_3$, 350.1751); UV λ_{max}(MeOH) nm (log ϵ): 252 (3.61), 265 (3.71), 281(2.68), 340 (2.61) and 355 (3.20); IR ν_{max} (NaCl) cm^{-1}: 3340, 1596, 1519; ^1H NMR ($CDCl_3$, 400 and 600 MHz) δ (ppm), ^{13}C NMR ($CDCl_3$, 125 MHz) δ (ppm) data (see Table 1).

Molecular Descriptors Calculation

The molecular properties of (*R*)-13aα-densiindolizidine were predicted through SwissADME server (http://www.swissadme.ch/index.php). The descriptors include volume, log-P, topological polar surface area, number of OH or NH, molecular weight, number of rotatable bonds, number of atoms, number of O or N, drug-likeness including G protein-coupled receptors ligand,

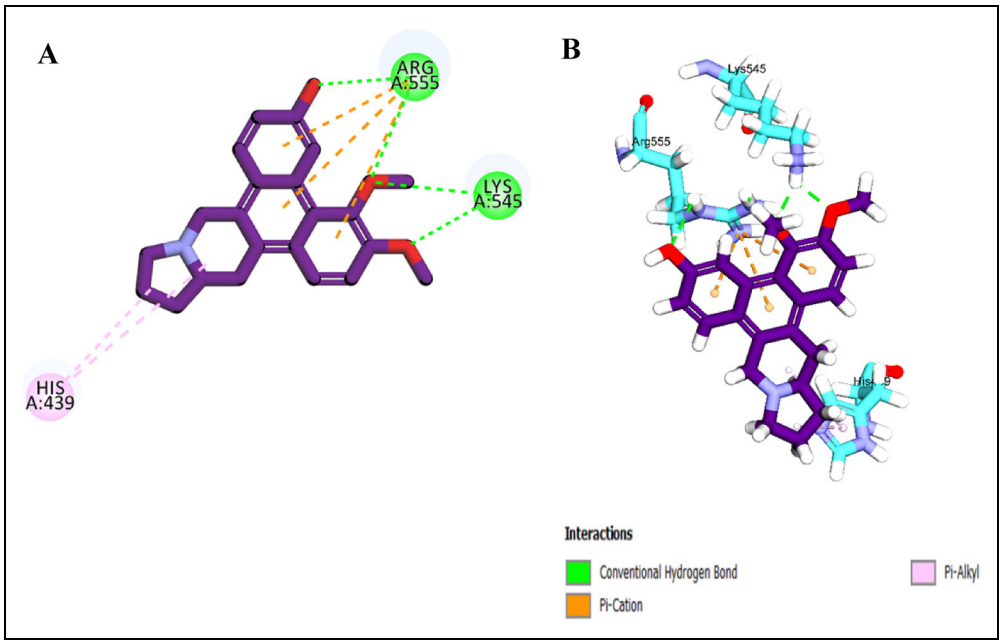

Figure 6. (A) 2D interaction of (*R*)-13aα-densiindolizidine at RNA primer strand of SARS-CoV-2 RdRp protein; (B) 3D interaction of (*R*)-13aα-densiindolizidine at RNA primer strand SARS-CoV-2 RdRp protein.

nuclear receptor ligand, a kinase inhibitor, ion channel modulator and the number of Lipinski's rule violations.

ADMET Prediction

The alkaloid (*R*)-13aα-densiindolizidine was subjected through ADMETlab (https://admet.scbdd.com/home/index/) for ADMET prediction. The prediction provides information about human intestinal absorption, atom-based logP (Alog P98), aqueous solubility, hepatotoxicity, blood–brain barrier, plasma protein binding, polar surface area, and cytochrome P450 2D6 (CYP2D6) descriptors.

Molecular Docking

In this work, SARS-CoV-2 RNA-dependent RNA-polymerase (RdRp) (PDB ID: 7D4F, 2.57 Å)[25] and main protease (M^{pro}) crystal structure complexed with inhibitor NS3 (PDB ID: 6LU7, 2.16 Å)[26] were retrieved from the Protein Data Bank (http://www.rcsb.org/).[27] Molecular docking was performed using CDOCKER module in Discovery Studio® (Accelrys). The co-crystallized ligands were first removed and then redocked with the protein binding site to validate the molecular docking protocol. Ligand binding pose were ranked based on their CDOCKER energy values.

Conclusions

Isolation, identification, and characterization of the compound isolated from the leaves of *C densiflora* yielded a new phenanthroindolizidine alkaloid named (*R*)-13aα-densiindolizidine. Since phenanthroindolizidine alkaloids are well known for their interesting pharmacological activities, thus the new alkaloid was subjected to *in silico* ADMET analyses. *In silico* findings suggest that the alkaloid could be a potent therapeutic lead as it fulfills Lipinski's rule criteria as well as the ability to properly bind and interact well with amino acid residues in the active site of SARS-CoV-2 M^{pro} and RdRp.

Acknowledgements

The authors would like to acknowledge the Department of Chemistry, Faculty of Science, the University of Malaya for the facilities and support of this work.

Declaration of Conflicting Interests

The authors declared no potential conflicts of interest with respect to the research, authorship, and/or publication of this article.

Funding

The authors disclosed receipt of the following financial support for the research, authorship, and/or publication of this article: This work was supported by the Univesriti Teknologi MARA, UiTM Dynamic Research (Grant No: 600-RMC/DINAMIK-POSTDOC 5/3-006/2020).

ORCID iDs

Wan N Nazneem Wan Othman https://orcid.org/0000-0001-8944-5724
Nor H Ismail https://orcid.org/0000-0002-2374-4630

Supplemental Material

Supplemental material for this article is available online.

References

1. De Kok RP. A revision of *Cryptocarya* R. Br. (Lauraceae) of Peninsular Malaysia. *Kew Bull*. 2016;71(1):1-26. doi:10.3767/000651916X693004
2. Ng FSP. Tree flora of Malaya. *Manual Forester*. 1989;4:132-1738.
3. Perry LM, Metzger J. *Medicinal plants of east and southeast Asia: Attributed properties and uses*. MIT press; 1980.
4. Timmermann BN, Valcic S, Liu YL, Montenegro G. Flavonols from *Cryptocarya alb*a. *Z Naturforsch, C, J Biosci*. 1995;50(11–12):898-899. doi:10.1515/znc-1995-11-1223
5. Dumontet V, Hung NV, Adeline MT, et al. Cytotoxic flavonoids and α-Pyrones from *Cryptocarya obovata*. *J Nat Prod*. 2004;67(5):858-862. doi:10.1021/np030510h
6. Xiong R, Jiang J, Chen Y. Cytotoxic lignans from *Cryptocarya impressinervia*. *Nat Prod Res*. 2021;35(6):1019-1023. doi:10.1080/14786419.2019.1611808
7. Usman H, Hakim EH, Harlim T, et al. Cytotoxic chalcones and flavanones from the tree bark of *Cryptocarya costata*. *Z Naturforsch, C, J Biosci*. 2006;61(3–4):184-188. doi:10.1515/znc-2006-3-405
8. Toribio A, Bonfils A, Delannay E, et al. Novel *seco*-dibenzopyrrocoline alkaloid from *Cryptocarya ouhatchensis*. *Org Lett*. 2006;8(17):3825-3828. doi:10.1021/ol061435f
9. Othman WNNW, Liew SY, Khaw KY, Murugaiyah V, Litaudon M, Awang K. Cholinesterase inhibitory activity of isoquinoline alkaloids from three *Cryptocarya* species (Lauraceae). *Bioorg Med Chem*. 2016;24(18):4464-4469. doi:10.1016/j.bmc.2016.07.043
10. Othman WNNW, Sivasothy Y, Liew SY, et al. Alkaloids from *Cryptocarya densiflora* Blume (Lauraceae) and their cholinesterase inhibitory activity. *Phytochem Lett*. 2017;21:230-236. doi:10.1016/j.phytol.2017.07.002
11. Mandhare AA, Dhulap SA, Dhulap AS, Biradar SC. Review on the anticancer and *in-silico* binding studies of phenanthroindolizidine alkaloids. *Chem Inform*. 2015;1(1):1-15. doi:10.21767/2470-6973.100005
12. Gellert E, Pelletier SW. *Alkaloids, chemical and biological perspectives*. Academic Press; 1987:55-132.
13. Ratnagiriswaran AN, Venkatachalam K. The chemical examination of *Tylophora asthmatica* and the isolation of the alkaloids tylophorine and tylophorinine. *Indian J Med Res*. 1935; 22:433-441.
14. Jia XH, Zhao HX., Du CL, Tang WZ, Wang X.J. Possible pharmaceutical applications can be developed from naturally occurring phenanthroindolizidine and phenanthroquinolizidine alkaloids. *Phytochem Rev*. 2021; 20(4):845-868. doi:10.1007/s11101-020-09723-3
15. Min HY, Chung HJ, Kim EH, Kim S, Park EJ, Lee SK. Inhibition of cell growth and potentiation of tumor necrosis factor-α (TNF-α)-induced apoptosis by a phenanthroindolizidine alkaloid antofine in human colon cancer cells. *Biochem Pharmacol*. 2010;80(9):1356-1364. doi:10.1016/j.bcp.2010.07.026
16. Yang CW, Lee YZ, Hsu HY, et al. Inhibition of SARS-CoV-2 by highly potent broad-spectrum anti-coronaviral tylophorine-based derivatives. *Front Pharmacol*. 2020:2056. doi:10.3389/fphar.2020.606097
17. Yang CW, Lee YZ, Kang IJ, et al. Identification of phenanthroindolizines and phenanthroquinolizidines as novel potent anti-coronaviral agents for porcine enteropathogenic coronavirus transmissible gastroenteritis virus and human severe acute respiratory syndrome coronavirus. *Antivir Res*. 2010;88(2):160-168. doi:10.1016/j.antiviral.2010.08.009
18. Yang CW, Lee YZ, Hsu HY, et al. Targeting coronaviral replication and cellular JAK2 mediated dominant NF-κB activation for comprehensive and ultimate inhibition of coronaviral activity. *Sci Rep*. 2017;7(1):1-3. doi:10.1038/s41598-017-04203-9
19. Gellert E. The indolizidine alkaloids. *J Nat Prod*. 1982;45(1):50-73. doi:10.1021/np50019a005
20. Damu AG, Kuo PC, Shi LS, et al. Phenanthroindolizidine alkaloids from the stems of *Ficus septica*. *J Nat Prod*. 2005;68(7):1071-1075. doi:10.1021/np050095o
21. Wu TS, Su CR, Lee KH. Cytotoxic and anti-HIV phenanthroindolizidine alkaloids from *Cryptocarya chinensis*. *Nat Prod Commun*. 2012;7(6):725-727. doi:10.1177/1934578X1200700608
22. Cave A, Leboeuf M, Moskowitz H, et al. Alkaloids of *Cryptocarya phyllostemon*. *Aust J Chem*. 1989;42(12): 2243-2263. doi:10.1071/CH9892243
23. Zhu W, Chen CZ, Gorshkov K, Xu M, Lo DC, Zheng W. RNA-dependent RNA polymerase as a target for COVID-19 drug discovery. *SLAS Discov: Adv Sci Drug Dis*. 2020;25(10):1141-1151. doi:10.1177/2472555220942123
24. Yin W, Luan X, Li Z, et al. Structural basis for inhibition of the SARS-CoV-2 RNA polymerase by suramin. *Nat Struct Mol Biol*. 2021;28(3):319-325. doi:10.1038/s41594-021-00570-0
25. Jin Z, Du X, Xu Y, et al. Structure of m^{pro} from SARS-CoV-2 and discovery of its inhibitors. *Nature*. 2020;582(7811):289-293. doi:10.1038/s41586-020-2223-y
26. Burley SK, Berman HM, Bhikadiya C, et al. RCSB Protein data bank: biological macromolecular structures enabling research and education in fundamental biology, biomedicine, biotechnology and energy. *Nucleic Acids Res*. 2019;47(D1):D464-D474. doi:10.1093/nar/gky1004
27. Wu G, Robertson DH, Brooks CLIII, Vieth M. Detailed analysis of grid-based molecular docking: a case study of CDOCKER—A CHARMm-based MD docking algorithm. *J Comput Chem*. 2003;24(13):1549-1562. doi:10.1002/jcc.10306